Phys. Med. Biol., 1992, Vol. 37, No 6, 1203–1217. Printed in the UK

Determination of optical properties of turbid media using pulsed photothermal radiometry

S A Prahl†, I A Vitkin‡, U Bruggemann†, B C Wilson‡ and R R Anderson†

† Wellman Research Laboratories of Photomedicine, Massachusetts General Hospital, Boston MA 02114, USA

‡ Hamilton Regional Cancer Centre and McMaster University, Department of Physics, Hamilton, Ontario, L8V 1C3 Canada

Received 10 September 1991

Abstract. Pulsed photothermal radiometry (PPTR) measures blackbody radiation emitted by a sample after absorption of an optical pulse. Three techniques for obtaining the absorption coefficient of absorbing-only, semi-infinite samples are examined and shown to give comparable results. An analytic theory for the time dependence of the PPTR signal in semi-infinite scattering and absorbing media has been derived and tested in a series of controlled gel phantoms. This theory, based on the diffusion approximation of the radiative transport equation, is shown to model the time course of the detected signal accurately. Furthermore, when the incident fluence is known, the theory can be used in a non-linear, two-parameter fitting algorithm to determine the absorption and reduced scattering coefficients of a turbid sample with an accuracy of 10–15% for transport albedos ranging from 0.42–0.88.

1. Introduction

Pulsed photothermal radiometry (PPTR) is a relatively new optical technique based on remote measurement of the temperature changes resulting from absorption of a short light pulse. The temperature is determined by measuring the black-body infrared (IR) emission from the sample under study. By analysing the PPTR signal, information about the thermal or the optical properties of the sample can be obtained. PPTR has been used as a method for depth analysis and non-destructive evaluation of the subsurface thermal properties (Imhof *et al* 1984, Leung and Tam 1984, Tam 1985). In studies of laminated or layered materials, PPTR is used to determine changes in the thermal property of a particular layer (Cielo 1984, Balageas *et al* 1986). Thermal parameters of homogeneous materials have also been determined in samples with known optical properties. The internal distribution light is used as the thermal source, and an analytic expression for the heat diffusion is obtained (Tam 1987). The materials are often coated with a thin, optically absorbing layer so that the heat is deposited exclusively at the surface.

Our goal was to start with the sample's thermal properties and use the thermal signal to determine the absorption and scattering properties. This extends previous PPTR studies that only included absorption in their analysis. For example, successful investigations have yielded the absorption characteristics of biliary calculi (Long *et*

0031-9155/92/061203+15$04.50

al 1987b), normal and diseased human arteries (Long and Deutsch 1987), and skin (Long *et al* 1987a). In this paper, we compare various methods for analysing the signal from an absorbing-only medium. One method requires a measurement of the incident fluence and the others use the shape of the temperature decay curve.

At most visible and near-infrared wavelengths, the optical properties of tissue have non-negligible scattering properties (Cheong *et al* 1990), and consequently, absorbing-only theories are inapplicable. Non-invasive methods for determining the optical absorption and scattering properties of tissues are of particular interest since this information has diagnostic and therapeutic value in photomedicine (Patchan *et al* 1991, Wilson 1991). Recently, Anderson *et al* (1989) have developed a model for evaluating the initial temperature rise in PPTR experiments on scattering and absorbing gels. Interpretation of PPTR signals required measurements of either the incident fluence and calibration factors, or the diffuse reflectance from the sample. In this paper, we derive a theory for the infrared emission from a scattering and absorbing (turbid) medium and test it using a series of turbid gel phantoms. We show that the results of Anderson *et al* (1989) are a special case of the new turbid medium theory. Furthermore, we give two new methods for obtaining optical properties of a turbid material—the first requires an additional measurement of the incident fluence and the second requires an additional diffuse reflection measurement. Finally, we give evidence that the temporal shape of the PPTR signal is insufficient to determine the optical properties of a turbid material uniquely, and that an additional measurement is necessary to select the correct value.

We used aqueous gel phantoms with known optical properties to test our algorithms. Water was used as the base medium because its thermal diffusivity is well known and is nearly equal to that of most soft tissues (Bowman *et al* 1975). The techniques for purely absorbing samples had errors less than 10% and those for scattering and absorbing samples had errors of 10–15%.

2. Theory

The photothermal radiometric signal results from the induced temperature rise in the material caused by the absorption of an incident pulse of optical irradiation (Leung and Tam 1984). The optical properties of the material and the irradiation geometry determine the spatial distribution of the optical energy in the material. The medium is assumed to have uniform optical and thermal properties, and all the absorbed optical energy is assumed to be converted directly to heat. In reality, some fraction may be lost to photochemical or photomechanical processes, and these may need to be accounted for in the energy balance, depending on the irradiation wavelength and medium. The optical irradiation is assumed normal to the slab. The irradiation is uniform and sufficiently wide that radial conduction is negligible. The medium is assumed to be semi-infinite, both optically and thermally. The rest of this section follows the work of Leung and Tam (1984).

The one-dimensional heat conduction equation describes the temperature of the sample,

$$\frac{\partial^2 T}{\partial z^2} = \frac{1}{\alpha}\frac{\partial T}{\partial t} \tag{1}$$

where T is the temperature, α is the thermal diffusivity of the sample, t is the time and z is zero at the surface and increases into the material. If we assume negligible

heat loss at the surface, we can use Green's functions and the method of images to solve (1) for the temperature in the sample (Carslaw and Jaeger 1986)

$$T(z,t) = \frac{1}{\sqrt{4\pi\alpha t}} \int_0^\infty T(z',0) \left[\exp\left(-\frac{(z-z')^2}{4\alpha t} \right) + \exp\left(-\frac{(z+z')^2}{4\alpha t} \right) \right] \mathrm{d}z' \quad (2)$$

where $T(z',0)$ is the initial temperature distribution that depends on the optical and thermal properties of the material, and on the incident light fluence.

The measured radiometric signal is obtained by integrating the Stefan–Boltzmann law over all depths weighted by the infrared attenuation in the material,

$$S(t) = \eta a_D \varepsilon \sigma \mu_{IR} \int_0^\infty [T(z,t)^4 - T_0^4] \exp(-\mu_{IR} z)\, \mathrm{d}z. \quad (3)$$

In this equation, T_0 is the uniform unperturbed sample temperature, η is the detector efficiency (incorporating both the sensitivity and collection efficiency of the detector), a_D is the detector area, ε is the emissivity of the sample, σ is the Stefan–Boltzmann constant, and μ_{IR} is the average absorption coefficient of the sample over the range of infrared wavelengths detected. This last quantity determines the depth into the sample from which contributions to the measured signal are obtained: if $\mu_{IR} \gg 1$, then most of the detected signal is radiated from points close to the surface; as $\mu_{IR} \to 0$, the signal disappears because the material is transparent in the infrared. If the temperature rise $(T(z,t) - T_0)$ is small, the bracketed quantity in (3) can be expanded using the binomial theorem. Neglecting terms of $O(T_0^2)$ and lower yields

$$S(t) = 4\eta a_D \sigma \varepsilon T_0^3 \mu_{IR} \int_0^\infty [T(z,t) - T_0] \exp(-\mu_{IR} z)\, \mathrm{d}z. \quad (4)$$

If $\mu_{IR} \to \infty$, then (4) becomes

$$S(t) = 4\eta a_D \sigma \varepsilon T_0^3 [T(0,t) - T_0] \quad (5)$$

implying that the signal is a direct measure of the surface temperature increase.

2.1. Homogeneous absorber

The light distribution in a homogeneous absorber is described by Beer's law (Born and Wolf 1980). Assuming normal incidence,

$$E(z) = E_{inc} \exp(-\mu_a z) \quad (6)$$

where $E(z)$ is the energy fluence, E_{inc} is the light fluence at the surface (the irradiance reduced by the any losses due to specular reflection from the surface), and μ_a is the optical absorption coefficient at the incident light wavelength. If all absorbed light is converted to heat, the initial temperature distribution is

$$T(z,0) = \frac{E_{inc}\mu_a}{\rho c} \exp(-\mu_a z) \quad (7)$$

where ρc is the volumetric specific heat of the sample. Substituting this distribution into (2), and using the resulting temperature field to solve (4) yields

$$S(t) = \frac{4\eta a_D \varepsilon \sigma T_0^3 E_{inc}}{\rho c} \frac{\mu_a \mu_{IR}}{\mu_{IR}^2 - \mu_a^2} [\mu_{IR} f(\mu_a^2 \alpha t) - \mu_a f(\mu_{IR}^2 \alpha t)] \quad (8)$$

where $f(x) = \exp(x)\mathrm{erfc}(\sqrt{x})$, and $\mathrm{erfc}(x)$ is the complementary error function of x (Carslaw and Jaeger 1986). The signal in (8) decays monotonically with time at a rate that depends on the optical and thermal properties of the sample. The IR absorption affects the net infrared emission from the sample and is important for estimating the surface temperature. Specifically, the maximum signal that corresponds to the initial temperature increase at $t = 0$,

$$S(0) = (4\eta a_D \varepsilon \sigma T_0^3)\left(\frac{E_{inc}\mu_a}{\rho c}\right)\frac{\mu_{IR}}{\mu_{IR} + \mu_a} \tag{9}$$

is affected by the relative sizes of μ_{IR} and μ_a. As discussed by Anderson *et al* (1989), when μ_{IR} is no longer much larger than μ_a, the last term in (9) is no longer unity and the detected signal is reduced accordingly. Furthermore, the signal also depends on the product $\mu_a\mu_{IR}$, and decreases as either parameter becomes small.

2.2. Homogeneous scattering and absorbing media

Many models of light transport in scattering and absorbing materials have been developed (Hansen and Travis 1974, Patterson *et al* 1990), varying from accurate numerical models to less accurate closed-form expressions. We shall use the diffusion approximation of the radiative transport equation because it retains the important features of light propagation in tissues (absorption, anisotropic scattering and mismatched boundary conditions) while remaining amenable to analytic manipulation. The diffusion approximation is generally accepted as accurate when scattering dominates absorption (Ishimaru 1978); however, when absorption dominates scattering, the diffusion solution reduces to Beer's law, and the diffusion approximation is again accurate. We proceed to derive the thermal response of a turbid medium assuming the diffusion approximation is valid for intermediate values as well, and will later experimentally test the accuracy of the derived result.

The solution for a one-dimensional, uniform, collimated beam normally incident on a semi-infinite optical slab is (Patterson *et al* 1990),

$$E(z) = A\exp(-\mu_{eff}z) + B\exp(-\mu_{tr}z) \tag{10}$$

with

$$A = \frac{E_{inc}(9 + 6k)\mu_s' D}{(1 + k\sqrt{4\mu_a D})(1 - 9\mu_a D)} \qquad B = \frac{-2E_{inc}}{1 - 9\mu_a D}$$

where $\mu_s' = \mu_s(1 - g)$ is the reduced scattering coefficient, g is the average cosine of the scattering angle, $\mu_{tr} = \mu_a + \mu_s'$ is the transport coefficient, k is a semi-empirical constant that depends on the refractive indices of the sample and surrounding medium, $D = (3\mu_{tr})^{-1}$ is the optical diffusion constant, and $\mu_{eff} = \sqrt{3\mu_{tr}\mu_a}$ is the effective attenuation coefficient. Notice that, in the limit of negligible scattering ($\mu_s \to 0$), $A \to 0$, $B \to E_{inc}$ and $\mu_{tr} \to \mu_a$, in agreement with (6).

The PPTR signal for a source corresponding to (10) is

$$S(t) = C\frac{\mu_a}{\rho c}\left[Af(\mu_{eff}^2\alpha t) + Bf(\mu_{tr}^2\alpha t)\right] \qquad \mu_{IR} \to \infty \tag{11}$$

where $C = 4\eta a_D \sigma \varepsilon T_0^3$ and we have assumed that the IR absorption coefficient is much larger than either μ_{tr} or μ_{eff}. When this is invalid the PPTR signal is given by

$$S(t) = C\frac{\mu_a \mu_{IR}}{\rho c}\left(\frac{A}{\mu_{IR}^2 - \mu_{eff}^2}[\mu_{IR} f(\mu_{eff}^2 \alpha t) + \mu_{eff} f(\mu_{IR}^2 \alpha t)] + \frac{B}{\mu_{IR}^2 - \mu_{eff}^2}[\mu_{IR} f(\mu_{tr}^2 \alpha t) + \mu_{tr} f(\mu_{IR}^2 \alpha t)]\right). \quad (12)$$

As in the case of a purely absorbing medium (8), the signal vanishes as either $\mu_a \to 0$ or as $\mu_{IR} \to 0$.

The effect of scattering on the PPTR signal is demonstrated in figure 1(*a*), which shows theoretical signal profiles derived from (12), for a fixed μ_a (47 cm^{-1}) and values of μ_s' ranging from 0–137 cm^{-1}. The corresponding fluence profiles, calculated from (10), are shown in figure 1(*b*). As scattering increases, the fluence near the surface increases and the initial temperature increases. This effect has been explained by Anderson *et al* (1989) using a heuristic argument based on the internal reflection of backscattered photons at the surface boundary. Their result was

$$E(0) = E_{inc}(1 + 2kR_d) \quad (13)$$

where R_d is the diffuse reflectance for the refractive index mismatched boundary condition. An equivalent result can be derived rigorously by evaluating (10) at $z = 0$

$$E(0) = A + B = E_{inc}\left[1 + 2k\left(\frac{a'}{1 + 2k(1-a') + (2k/3)\sqrt{3(1-a')}}\right)\right] \quad (14)$$

where the transport albedo is

$$a' = \frac{\mu_s'}{\mu_a + \mu_s'}.$$

The quantity in the curly brackets is the diffuse reflectance as predicted by diffusion theory (Flock *et al* 1989).

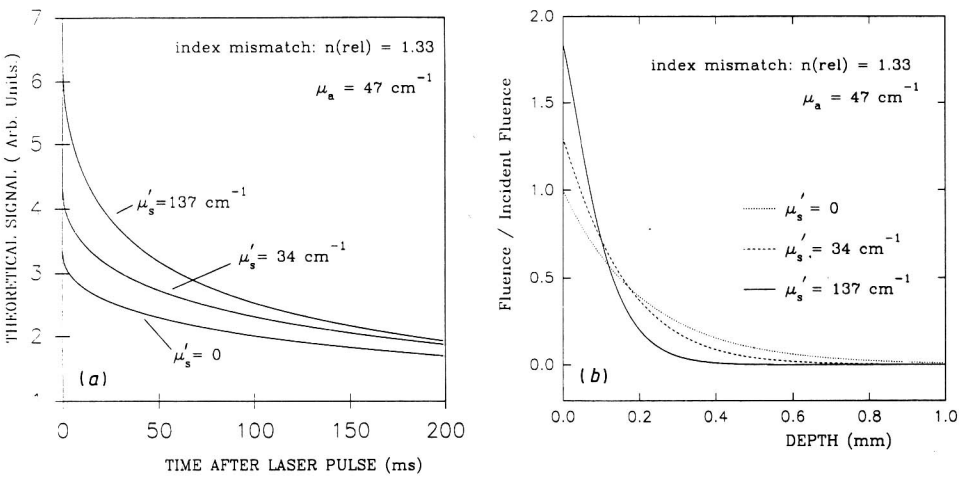

Figure 1. (*a*) The effect of scattering on the PPTR signal. Theoretical profiles for a fixed $\mu_a = 47$ cm^{-1} and various μ_s' obtained using (12) and a fixed incident fluence. (*b*) The corresponding fluence distributions in the sample.

A. Diffuse Light

Consider light incident upon the side of the wall of the reflectance sphere (Fig. 2A) as in Subsection 2.A and rewrite Eq. (14) as

$$P_{d1} = \frac{\delta}{A}\frac{m}{V}P, \tag{24}$$

where

$$V = 1 - \left(m\alpha + R_d\frac{s}{A} + r\frac{\delta}{A}\right) \tag{25}$$

and where the subscript 1 has been added to P_d to indicate that this power is only part of the total power detected. It is the power incident upon the detector surface within the reflectance sphere that is due only to the light generated within the reflectance sphere that has not traveled through the sample from the transmittance sphere.

Since P_{d1} is the power incident upon the detector of surface area δ, we may deduce that

$$P_{s1} = \frac{s}{A}\frac{m}{V}P \tag{26}$$

is the power incident upon the sample.

We know that this power (P_{s1}) multiplied by the coefficient for the diffuse transmission of diffuse incident light (T_d) will provide a source for the transmittance sphere, as in expression (19), such that there is a power incident upon the detector in the transmittance sphere of

$$P_{d1}' = \frac{\delta'}{A'}\frac{1}{V'}T_dP_{s1} = \frac{\delta'}{A'}\frac{T_d}{V'}\frac{s}{A}\frac{m}{V}P, \tag{27}$$

where V' is identical to V in nomenclature except that it and the other appropriate sphere parameters have been changed (prime added) to account for the possibility of the transmittance sphere's being different from the reflectance sphere.

A fraction of light transmitted into the transmittance sphere is incident back upon the sample,

$$P_{s1}' = \frac{s}{A'}\frac{1}{V'}T_dP_{s1}, \tag{28}$$

and acts as a second source for the reflectance sphere ($P_{s1}'T_d$) such that the detector detects an additional power of

$$P_{d2} = \frac{\delta}{A}\frac{1}{V}T_dP_{s1}' = \frac{\delta}{A}\frac{m}{V}\frac{T_d}{V}\frac{T_d}{V'}P. \tag{29}$$

Similarly some of this second source is incident back upon the sample and is transmitted. This light acts as a second source in the transmittance sphere.

This process of the exchange of light between the two spheres continues *ad infinitum*, and the total light incident upon the detectors may be calculated as a sum of a geometric series of the power detected for each source (each exchange of light) within each sphere to give, for the reflectance sphere, a total detected power of

$$P_d = \frac{\delta}{A}\frac{m}{V}\frac{1}{1 - TT'}P \tag{30}$$

and, for the transmittance sphere, a total detected power of

$$P_d' = \frac{\delta'}{A'}\frac{s}{A}\frac{mT_d}{V}\frac{1}{V'}\frac{1}{1 - TT'}P, \tag{31}$$

where

$$T = \frac{s}{A}\frac{T_d}{V} \tag{32}$$

and

$$T' = \frac{s}{A'}\frac{T_d}{V'}. \tag{33}$$

The calculations described here are summarized in Table 3, where Eqs. (30) and (31) may be calculated by summing columns 3 and 5, respectively.

B. Collimated Light

If collimated light is first incident upon the sample within the reflectance sphere, then we may calculate the power detected in each sphere by using procedure identical to that in Subsection 3.A but now with two initial sources in the reflectance sphere [expressions (16) and (17)] and two in the transmittance sphere [expressions (20) and (21)]. Combining these expressions with Eqs. (30) and (31) yields the following results.

For the reflectance sphere the total detected power will be

$$P_d = \frac{\delta}{A}\frac{[R_{cd} + mR_c + T'(T_{cd} + m'T_c)]}{V(1 - TT')}P, \tag{34}$$

and for the transmittance sphere the total detected power will be

$$P_d' = \frac{\delta'}{A'}\frac{[T_{cd} + mT_c + T(R_{cd} + mR_c)]}{V'(1 - TT')}P. \tag{35}$$

C. Discussion of the Sphere Equations

The equations for the power detected in the double-sphere system [Eqs. (30), (31), (34), and (35)] may be understood in terms of the equations for the single-sphere systems [Eqs. (14), (18), (22), and (23)] and in terms of the sources of diffuse light.

To explain the equations, we use the example of a collimated source. In the single- and the double-sphere cases for reflected light there are two diffuse-light sources,

$$R_{cd}P, \tag{36}$$

$$mR_cP. \tag{37}$$

In the double-sphere case there is a third source of diffuse light that is due to a proportion of the collimated light first incident upon the sample that is transmitted through the sample into the transmittance sphere. Some of this

The infrared emission from the sample was monitored at normal incidence using a 1 mm^2 liquid-nitrogen cooled HgCdTe radiation detector (New England MPC 12-1-8) placed at the focal plane of a germanium lens. The detection bandwidth was 3–12 μm, thus capturing about 40% of the spectral emission emanating from the heated gels (Ozisik 1985). The germanium lens was used in a 1:1 conjugate ratio to provide a 1 mm^2 detector viewing area at the centre of the irradiated sample surface. For measurements of incident fluence, a known fraction of light exiting the fibre was diverted to an energy meter (Gentec ED200) by a beam splitter. The electrical response of the detector, after pre-amplification, was monitored with a 125 MHz digital oscilloscope (LeCroy 9400A), triggered from the output of a silicon photodiode (EG&G FND-100) which detected the stray light from the dye laser flashlamp. Typically, the sampling rate of the digital oscilloscope was 8 μs/point, and infrared signals were recorded for 180 ms after the laser pulse. All reported measurements are for a single light pulse. The recorded signal was reduced to 200–400 points by averaging. The stability of the measuring apparatus was checked periodically by observing the signal from a neutral density filter (Schott NG-10).

For system calibration, we measured the detector voltage as a function of the temperature of a copper block coated with lampblack and heated by a resistive heater. The temperature was measured using a precision thermistor (Omega 44031) embedded in the block. For improved signal to noise ratio, lock-in detection was used, with the signal representing the difference between the thermal emission from the room-temperature optical chopper blade and from the heated copper surface. For temperature increases of 5–60 °C, the lock-in amplifier (Stanford Research Systems SR500) voltage was proportional to the copper block temperature, with a ratio of 6.3 ± 0.2 mV $°C^{-1}$.

4. Results and analysis

4.1. Absorbing gels

A typical thermal response of a purely absorbing gel phantom ($\mu_a = 40$ cm^{-1}) following a 1 μs, 300 mJ cm^{-2} laser pulse at 627 nm is shown in figure 3. A rapid temperature jump followed by a monotonic decay is seen. The initial temperature increase was moderate and in subsequent experiments ranged from 5 °C for the lowest absorbing gels to 15 °C for the highest absorbing and scattering gels.

The absorption coefficient of a purely absorbing gel may be determined from the initial signal, a fluence measurement and several calibration factors by using (9). The bracketed quanities in (9) are known from calibration. The infrared absorption ($\mu_{IR} = 1200$ cm^{-1}) was the average value of the infrared absorption of water weighted by the detector sensitivity. The specific heat of water per unit volume ($\rho c = 4.184$ J cm^{-3} $°C^{-1}$) was used for the gels. Using these values, PPTR measurements can be interpreted using (9). The results are shown in column A of table 1, with the errors determined from experimental uncertainties. The slight overestimation probably results from errors in measuring the laser spot size.

This initial-temperature method ignores potentially useful information at later times in the temperature signal. Furthermore, additional measurements are needed to interpret the results (calibration curve, fluence measurements). Two alternative approaches, which used the temporal response from the sample, were developed to

Table 1. Absorption values for absorbing-only samples assuming $\mu_{IR} = 1200\,cm^{-1}$. The 'true' values were obtained spectrophotmetrically. Column (A) was determined from the analysis of the peak height and the calibration curve information (9); the error is based on uncertainties in the peak height, μ_{IR}, the incident fluence and the calibration slope. Column (B) was determined using (15); the error is the standard deviation on the interval 0–180 ms. Column (C) was determined from the minimum in the response surface; the typical error of 10% is estimated from the surface topology. All values are given in units of cm^{-1}.

'True' μ_a	(A) Peak height	(B) Normalization	(C) Two-parameter
144	137 ± 23	147 ± 9	137 ± 14
117	125 ± 21	104 ± 7	104 ± 10
93	102 ± 17	92 ± 5	87 ± 9
70	73 ± 12	71 ± 4	71 ± 7
46	52 ± 8	49 ± 4	49 ± 5
23	30 ± 5	21 ± 6	21 ± 2

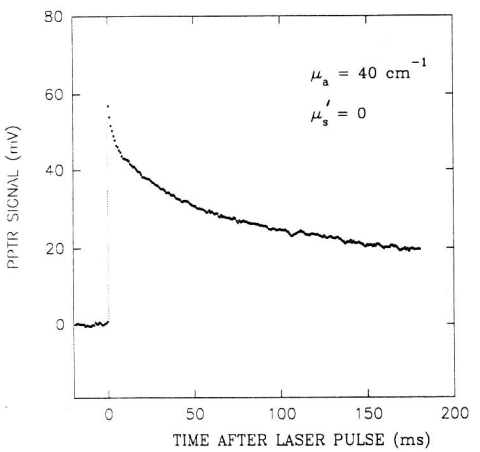

Figure 3. Typical PPTR signal from a homogeneous absorbing-only gel ($\mu_a = 40\,cm^{-1}$). The incident fluence was 400 mJ cm^{-2}.

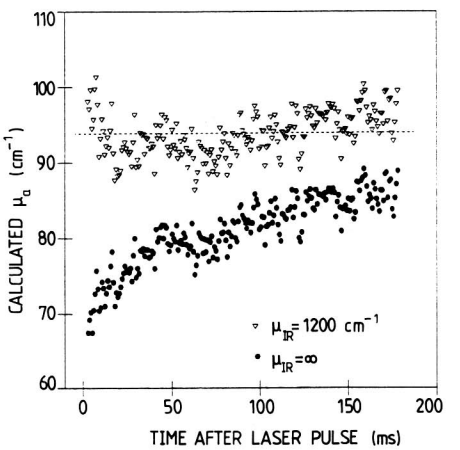

Figure 4. Results using (15) to determine the absorption coefficient from an experimental PPTR profile at any t. The true absorption value is indicated by the horizontal line $\mu_a = 93\,cm^{-1}$. The derived value (average over all times) is $92 \pm 5\,cm^{-1}$ for $\mu_{IR} = 1200\,cm^{-1}$ and $81 \pm 9\,cm^{-1}$ for $\mu_{IR} = \infty$.

find the absorption coefficient of absorbing-only gels. These eliminated the need for an incident fluence measurement.

The first method will be called the normalization method, because the thermal signal is normalized by its initial value. Dividing the temporal signal in (8) by the initial value from (9) creates a quantity independent of incident fluence and other calibration factors

$$\frac{S(t)}{S(0)} = \frac{\mu_{IR} f(\mu_a^2 \alpha t) - \mu_a f(\mu_{IR}^2 \alpha t)}{\mu_{IR} - \mu_a}. \tag{15}$$

The only unknown remaining is the absorption coefficient, which can be determined

for any particular time t. Assuming a thermal diffusivity for the gels which is equal to that of water ($\alpha = 0.0013\,\mathrm{cm^2\,s^{-1}}$), allows the absorption coefficient to be calculated as a function of time for each sample. Figure 4 shows results for a phantom with a true absorption coefficient of $\mu_a = 93\,\mathrm{cm^{-1}}$, assuming both finite and infinite values for the infrared absorption coefficient. Surprisingly, the derived values of μ_a are strongly affected by letting $\mu_{IR} \to \infty$, even though μ_{IR} is larger than μ_a by an order of magnitude in this example. The averaged μ_a values for several gels are displayed in column B of table 1.

The normalization method depends on accurate early-time measurements. To avoid this, a more general method based on a non-linear two-parameter fit was developed. The two-parameter method will also be used later in the more challenging turbid-media problem. Equation (8) can be rewritten to show explicitly that the signal only depends on the parameters K and μ_a,

$$S(t) = K\frac{\mu_a\mu_{IR}}{\mu_{IR}^2 - \mu_a^2}\left[\mu_{IR} f(\mu_a^2\alpha t) - \mu_a f(\mu_{IR}^2\alpha t)\right]. \tag{16}$$

Here the scaling multiplier $K = 4\eta a\sigma\varepsilon T_0^3 E_{inc}/\rho c$ represents a system calibration constant $4\eta a\sigma T_0^3$, multiplied by a sample-specific factor $\varepsilon E_{inc}/\rho c$. We again assume that $\alpha = 0.0013\,\mathrm{cm^2\,s^{-1}}$ and $\mu_{IR} = 1200\,\mathrm{cm^{-1}}$. The residual for any parameter pair (K, μ_a) is defined as the sum of the squares of the differences between the calculated and measured values of $S(t)$. The minimum residual determines a unique pair (K, μ_a) and therefore the absorption coefficient. A non-linear least-residual search routine with the variables μ_a and K was written, using an algorithm described by Bevington (1969). The convergence criterion was a change in residuals of less than 1 part in 5000. If the best-fit values are now used to calculate a residual for $S(t) \pm \Delta S$ (ΔS being the experimental uncertainty of the signal), then the range of parameter pairs with residuals between the minimum residual and the residual for $S(t) \pm \Delta S$ is an error estimate for the fitted values. For signal errors of $\Delta S = 3$ mV, the error in the fitted values is about 10%.

An example of a least-residuals calculation is displayed in the contour plot of figure 5 for a gel with $\mu_a = 70\,\mathrm{cm^{-1}}$. The minimum corresponds to $\mu_a = 71\,\mathrm{cm^{-1}}$. The inner-most contour approximately represents the $S(t) \pm \Delta S$ residual level: the possible range of μ_a is about 66–78 $\mathrm{cm^{-1}}$, which is conservatively specified as $\mu_a = 71 \pm 7\,\mathrm{cm^{-1}}$. All residuals were calculated over a 3–125 ms time interval; the early times were avoided because of electrical noise from the laser; later times were discarded because the signal was dominated by thermal diffusivity and contains relatively little optical information (Leung and Tam 1984). The use of the full 0–180 ms interval gives (K, μ_a) minima that differ by only 3–4% from the windowed values. The 3–125 ms time interval was used for the results presented in column C of table 1.

The derived values of K (scaled to the appropriate fluence E_{inc}) can be used in the analysis of the turbid gel problem, since K/E_{inc} represents an experimental calibration factor common to all the phantoms. For the gels used in table 1, K/E_{inc} was nearly constant (±3%).

4.2. Absorbing and scattering gels

The PPTR signal for a scattering and absorbing gel is given by (12) and depends on K, μ_a, μ_s', α and μ_{IR}. If we assume constant values for the diffusivity α and

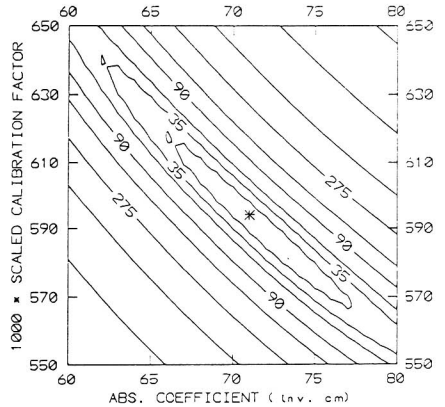

Figure 5. The residual contour surface used for the two-parameter fit of (16) to PPTR signals from an absorbing-only gel ($\mu_a = 70\,\mathrm{cm}^{-1}$). The location with the smallest residual is marked by an asterisk (μ_a, K) = ($71\,\mathrm{cm}^{-1}$, 0.593), and represents the best fit to the experimental data.

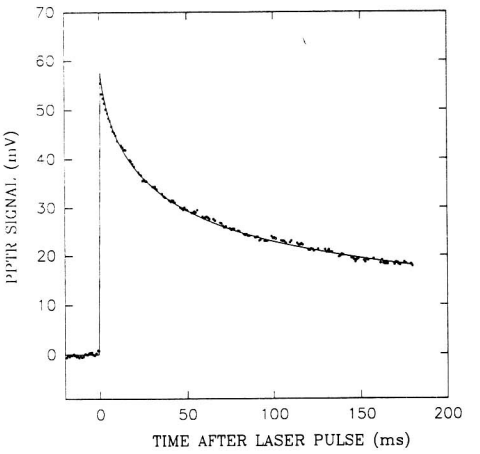

Figure 6. Theoretical PPTR profile, using (12) and the derived optical interaction coefficients (line), and experimental data (symbols). The data are from a gel with $\mu_a = 40\,\mathrm{cm}^{-1}$, $\mu_s' = 150\,\mathrm{cm}^{-1}$; the derived values used to generate the solid line are $\mu_a = 38\,\mathrm{cm}^{-1}$, $\mu_s' = 156\,\mathrm{cm}^{-1}$.

μ_{IR}, then the PPTR signal only depends on three parameters. The dependence can be reduced to two parameters by using the calibration constant K/E_{inc} obtained from the absorbing-only gels and measuring the incident fluence relative to that used for those gels. The two-parameter algorithm discussed above can now be used for analysing the PPTR signal from turbid gels, except that now (μ_a, μ_s') is varied and (12) is used in place of (9) to find the residuals. In figure 6, the measured PPTR signal is shown together with the theoretical prediction using (μ_a, μ_s') obtained from the two-parameter fit.

The results for a range of turbid gels are displayed in table 2. The 'true' values for the absorption coefficient were determined spectrophotometrically and the 'true' reduced scattering coefficients were calculated from Mie theory. The relative errors between these values and those derived using the non-linear two-parameter fit are ~10–15% and are roughly equal for transport albedos ranging from 0.42–0.88 (figure 7). The small relative errors in the intermediate albedo range ($\mu_a \approx \mu_s'$) are especially encouraging, since present theoretical constructs are generally ineffective in this regime (Wilson 1991).

A sensitivity analysis revealed that the calculated signal $S(t)$ was most sensitive to changes in the absorption coefficient. This is perhaps not surprising: while the optical distribution is sensitive to changes in both μ_a and μ_s', it is the absorption coefficient that governs the conversion of the optical fluence to heat, which is what is ultimately measured. Systematic changes in the thermal diffusivity and IR absorption coefficient, as well as in the time interval used for analysis, did not alter the location of the minimum residual significantly. Some changes in the μ_s' coordinate of the solution did occur, especially in response to thermal diffusivity variations. The μ_a coordinate of the solution was essentially unaffected. For example, changing the thermal diffusivity from 0.0013 to 0.0010 $\mathrm{cm}^2\,\mathrm{s}^{-1}$ shifted μ_s' by 15%, and μ_a by less

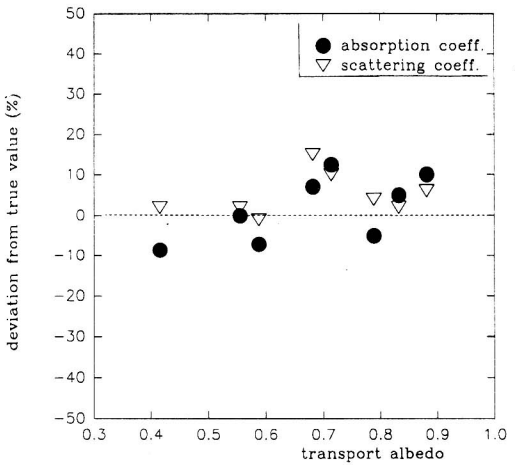

Figure 7. Percentage deviation (from true values) of μ_a and μ_s' derived from the analysis of turbid gels; see also table 2.

Table 2. Results of the two-parameter fit of (12) to PPTR signals from various turbid media. Typical errors in the scattering and absorption coefficients of about 10% are estimated from the topology of the least-residual surface near the convergence point. All values are given in units of cm^{-1}.

μ_a		μ_s'	
'True'	'Derived'	'True'	'Derived'
20	21	100	102
20	22	150	159
40	40	50	51
40	45	100	110
40	38	150	156
70	64	50	51
70	65	100	99
70	75	150	173

than 5%. We thus conclude that the PPTR signal is primarily dependent on μ_a, and is affected to a lesser extent by changes in the thermal diffusivity and μ_s'.

If the calibration constant K/E_{inc} is unknown then a three-parameter fit is an obvious choice for finding the three unknown parameters. Unfortunately, an arbitrary PPTR signal does not yield a unique triplet (μ_a, μ_s', K). For example, if the residuals for a fixed point (μ_a, μ_s') are minimized by optimizing K, then a contour plot similar to figure 8(*a*) is obtained. The valley, which includes the true value, also permits a multiplicity of solutions (μ_a, μ_s'): each point corresponds to a different value for K. Physically, this implies that different optical distributions will yield similar PPTR signals when irradiated by suitably chosen input fluences (figure 8(*b*)). Thus, it appears that the signal shape alone is insufficient to determine the absorption and the reduced scattering coefficients uniquely. Therefore, if a calibration coefficient is not available, an additional measurement is needed to determine the scattering and absorption coefficients of the material. A convenient additional measurement is the diffuse reflectance of the sample, which specifies the transport albedo and therefore

possibly be used to convert reflection values to transport albedos when the diffusion approximation is valid.

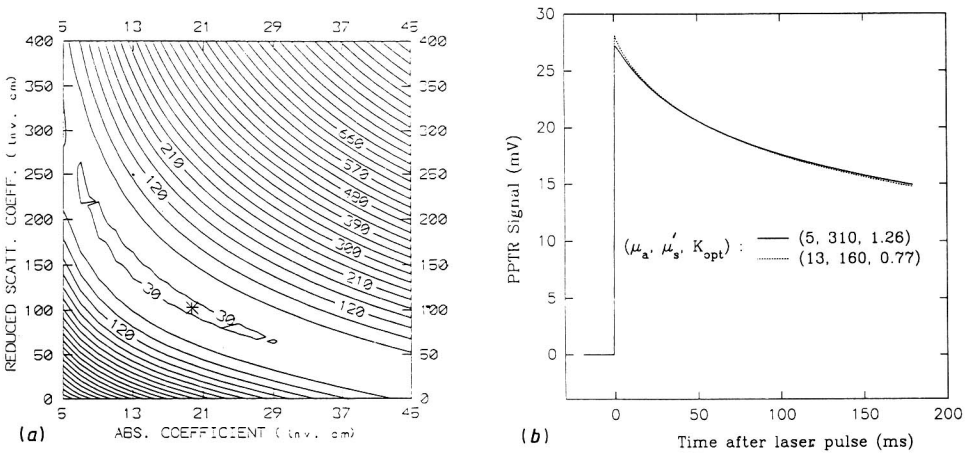

Figure 8. (*a*) Least-residual contour surface for a turbid gel. The true optical properties, $\mu_a = 20\ cm^{-1}$ and $\mu_s' = 100 cm^{-1}$, are indicated by an asterisk. For each point (μ_a, μ_s'), K is optimized to obtain a minimum residual. No unique minimum residual exists, implying a multiplicity of acceptable solutions. (*b*) Two theoretical PPTR profiles generated using two sets of triplets (μ_a, μ_s', K_{opt}) from the minimum residual valley of figure 8(*a*).

5. Discussion

The time profile of the infrared response of a sample to a light impulse is governed by its optical and thermal properties: the former determine the distribution of the optical energy, while the latter dictate the spatial and temporal behaviour of the resultant temperature field. If the thermal characteristics are known, a photothermal technique such as PPTR can be a useful non-invasive, non-contact method for probing the optical properties of turbid materials such as biological specimens.

Three methods for obtaining the absorption coefficients in semi-infinite absorbing-only gels are compared. In table 1 the accuracy of the initial peak and normalization methods is as good as that of the two-parameter fit method. This probably indicates consistent experimental technique for this set of absorbing samples. However, any noise in the early signal renders these approaches ineffective, and in such cases the more general and robust two-parameter fit must be used. Such a method does not depend more strongly on the early signals than on later signals, and therefore is relatively insensitive to noise in the early signal.

The PPTR response from a scattering medium can be used to determine the absorption and reduced scattering coefficients when the scaled calibration constant K/E_{inc} is known, using (12). This ratio is available from the two-parameter fit analysis using absorbing-only gel phantoms. Alternatively, the ratio could have been determined from the system calibration information, the sample's volumetric specific heat and the incident fluence. However, if this ratio is unknown, some useful optical

information can be obtained from the PPTR signal alone, simply by finding the optimum K value for each (μ_a, μ_s'). This approach selects many possible combinations of optical coefficients that lead to a similar minimum residual; additional information is needed to specify them uniquely.

A promising experimental stategy for this purpose is to measure the diffuse reflectance R_d. This measurement, together with the relative increase in the initial signal level, might serve as a check of the diffusion approximation used to derive (12). Such an increase in the initial signal level was observed experimentally, but an independent measurement of R_d would determine if the increase is in quantitative agreement with (13). More importantly, however, knowing the diffuse reflectance will provide the additional optical constraint that, in combination with the least-squares fit to the PPTR signal, should lead to a unique pair of (μ_a, μ_s') values. This would obviate the need to know the system calibration curve and the absolute incident fluence, both awkward measurements to perform accurately.

The turbid medium PPTR signal analysis depends on the applicability of the diffusion approximation to the material under study. This is not a restrictive assumption for many homogeneous mammalian tissues (e.g., liver, brain, breast) in the red and near-infrared (600–1110 nm). In this region scattering events are much more probable than absorption events, and the diffusion approximation is appropriate. Given that the optical diffusion model reduces to Beer's law in the limit of negligible scattering, the validity of our formulation can apply to absorption-dominated regions of the optical spectrum as well. This agreement has been verified for transport albedos ranging from 0.42–0.88.

6. Conclusion

Pulsed photothermal radiometry can be used to measure the optical properties of samples with known thermal properties. The analysis of the PPTR signals from absorbing-only media has been extended to eliminate the need for the relatively difficult measurement of the absolute value of the fluence of the light pulse. These methods are accurate to about 10% for absorption coefficients ranging from 20–140 cm^{-1}.

An analytic theory for the time dependence of the PPTR signal in semi-infinite scattering and absorbing media has been derived and tested in a series of controlled gel phantoms. In materials with scattering, either the incident fluence or another measurement characterizing the optical properties (e.g., diffuse reflectance) is needed to specify uniquely the absorption and scattering coefficients of a turbid medium. We have shown that when the incident fluence is known, the theory can be used in a non-linear two-parameter fitting algorithm to determine the optical properties of a turbid sample with an accuracy of 10–15% for transport albedos ranging from 0.42–0.88. Even in the absence of additional experimental information, the close agreement between theoretical profiles and experimental data suggests that the important physics of PPTR in turbid media have been included in our model.

Optothermal techniques should compliment purely optical methods because they are sensitive to *absorbed* radiation (higher absorption means a greater PPTR signal). In contrast, diffuse reflection decreases as the sample absorption increases. A combination of diffuse reflectance and PPTR measurements may prove useful for non-contact, non-invasive, *in vivo* measurement of the optical properties of scattering and absorbing tissues.

Acknowledgments

The authors thank Tom Farrell and Mike Patterson for helpful discussions. One of us (IAV) acknowledges the support of National Scioences and Engineering Research Council of Canada. This work was supported by Office of Naval Research Contract No. N00014-86-K-0117, NIH Grant No. 5R01AR25395-11, and the Ontario Laser and Lightwave Research Centre.

Résumé

Détermination des propriétés optiques des milieux troubles à l'aide de radiométrie photothermique pulsée.

La radiométrie photothermique pulsée (PPTR) mesure l'émission du corps noir issue d'un échantillon après absorption d'une impulsion optique. Les auteurs ont examiné trois techniques utilisables pour l'obtention des coefficients d'absorption d'échantillons uniquement absorbants et semi-infinis, et ont montré qu'elles conduisaient à des résultats comparables. Ils en ont déduit une théorie analytique de la variation en fonction du temps du signal PPTR dans les milieux absorbants et diffusants semi-infinis, qu'ils ont testée sur une série de gels fantômes contrôlés. Les auteurs ont montré que cette théorie, reposant sur l'approximation de la diffusion de l'équation du transport radiatif, modélisait exactement l'évolution au cours du temps du signal détecté. De plus, quant la fluence incidente est connue, la théorie peut être utilisée dans un algorithme d'ajustement non-linéaire à deux paramètres pour déterminer les coefficients d'absorption et de diffusion réduite d'un échantillon trouble avec une exactitude de 10 à 15% pour des albédos de transport s'étalant de 0.42 à 0.88.

Zusammenfassung

Bestimmung der optischen Eigenschaften dickflüssinger Medien mit Hilfe gepulster photothermischer Radiometrie.

Bei der gepulsten photothermischen Radiometrie (PPTR) wird die von einem schwarzen Körper emittierte Strahlung nach Absorption eines optischen Pulses gemessen. Drei Verfahren zur Ermittlung des Absorptionskoeffizienten von nur-absorbierenden, halb-unendlichen Proben wurden untersucht und führten zu vergleichbaren Ergebnissen. Eine analytische Theorie für die Zeitabhängigkeit des PPTR-Signals in halb-unendlichen Streu- und Absorptionsmedien wurde entwickelt und getestet in einer Reihe spezieller Gel-Phantome. Diese Theorie, die auf der Diffusionsnäherung der Strahlungstransportgleichung basiert, ist in der Lage, den zeitlichen Verlauf des nachgewiesenen Signals genau zu modellieren. Desweiteren kann die Theorie, wenn die einfallende Fluenz bekannt iust, in einem nicht-linearen zwei-parametrischen Anpassungsalgorithmus verwendet werden, um die Absorptions-und reduzierten Streukoeffizienten einer dickflüssigen Probe mit einer Genauigkeit von 10–15% für Transport-Albedos zwischen 0.42 und 0.88 zu bestimmen.

References

Anderson R R, Beck H, Bruggemann U, Farinelli W, Jacques S and Parrish J A 1989 Pulsed photothermal radiometry in turbid media: Internal reflection of backscattered radiation strongly influences optical dosimetry *Appl. Optics* **28** 2256–62

Ashtrahan M A 1979 Concerning hyperthermia phantom *Med. Phys.* **6** 235

Balageas D L, Krapez J C and Cielo P 1986 Pulsed photothermal modeling of layered materials *Appl. Optics* **59** 348–57

Bevington P R 1969 *Data Reduction and Error Analysis for the Physical Sciences* (New York: McGraw-Hill)

Bohren C F and Huffman D R 1983 *Absorption and Scattering of Light by Small Particles* (New York: Wiley)

Born M and Wolf E 1980 *Principles of Optics* (New York: Pergamon)

Bowman H F, Cravalho E G and Woods M 1975 Theory, measurement and application of thermal properties of biomaterials *Ann. Rev. Biophys. Bioeng.* **4** 43–80

Carslaw H S and Jaeger J C 1986 *Conduction of Heat in Solids* second edn (Oxford: Clarendon)

Cheong W F, Prahl S A and Welch A J 1990 A review of the optical properties of biological tissues *IEEE J. Quantum Electron.* **26** 2166–85

Cielo P 1984 Pulsed photothermal evaluation of layered materials *J. Appl. Phys.* **56** 230–4

Flock S T, Patterson M S, Wilson B C and Wyman D R 1989 Monte Carlo modeling of light propagation in high scattering tissue—I: Model predictions and comparison with diffusion theory *IEEE Trans. Biomed. Eng.* **BME-36** 1162–8

Hansen J E and Travis L D 1974 Light scattering in planetary atmospheres *Space Sci. Rev.* **16** 525–610

Imhof R E, Birch D J S, Thornley F R, Gilchrist J R and Strivens T A 1984 Optothermal transient emission radiometry *J. Phys. E: Sci. Instrum.* **17** 521–5

Ishimaru A 1978 *Wave Propagation and Scattering in Random Media* vol 1 (New York: Academic)

Leung W P and Tam A C 1984 Techniques of flash radiometry *J. Appl. Phys.* **56** 153–61

Long F H, Anderson R R and Deutsch T F 1987b Pulsed photothermal radiometry for depth profiling of layered media *Appl. Phys. Lett.* **51** 2076–8

Long F H and Deutsch T F 1987 Pulsed photothermal radiometry of human artery *IEEE J. Quantum Electron.* **QE-23** 1821–6

Long F H, Nishioka N S and Deutsch T F 1987a Measurement of the optical and thermal properties of biliary calculi using pulsed photothermal radiometry *Lasers Surg. Med.* **7** 461–6

Ozisik M N 1985 *Heat Transfer—A Basic Approach* (New York: McGraw-Hill)

Patchan M W 1991 Medical applications call for selectivity in laser performance *Laser Focus World* **4** 85–104

Patterson M S, Wilson B C and Graff R 1990 In vivo tests of the concept of photodynamic threshold dose in normal rat liver photosensitized by aluminum chlorosulphonated phthalocyanine *Photochem. Photobiol.* **51** 343–9

Tam A C 1985 Pulsed photothermal radiometry for noncontact spectroscopy, material testing and inspection measurements *Infrared Phys.* **25** 305–13

Tam A C 1987 Pulsed laser photoacoustic and photothermal detection *Photoacoustic and Thermal Wave Phenomena in Semiconductors* ed A Mandelis (New York: North-Holland) pp 175–99

Wilson B C 1991 Modelling and measurements of light propagation in tissue for diagnostic and therapeutic applications *Laser Systems for Photobiology and Photomedicine* ed A N Chester (New York: Plenum) pp 13–27